

EXTRACTING LONG-TERM TRENDS IN GEOMAGNETIC DAILY-VARIATIONS AND INDICES

Brian Hamilton (bham@bgs.ac.uk), Susan Macmillan
British Geological Survey, West Mains Road, Edinburgh EH9 3LA, United Kingdom

Abstract

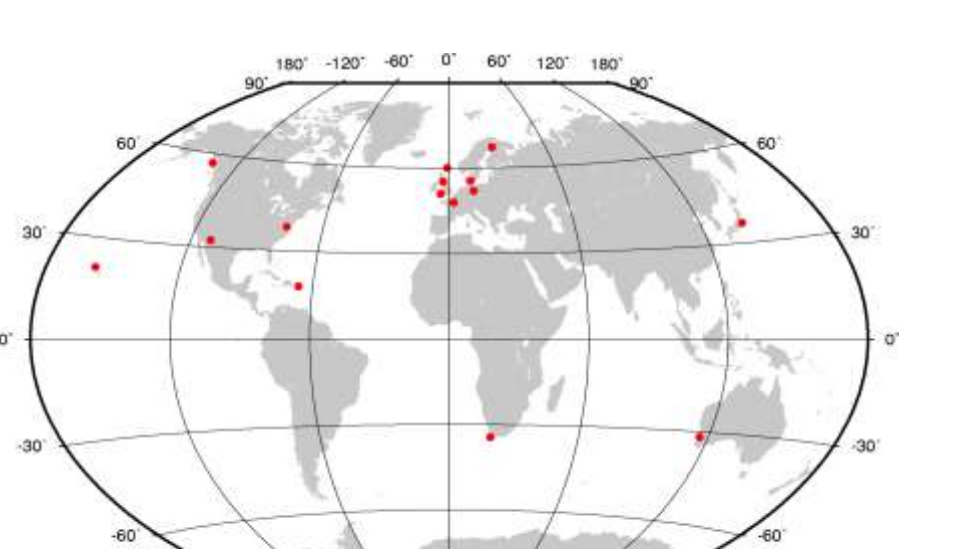
Long-term changes in the Earth's magnetic environment are of interest to those studying space weather and climate change and could act as proxies for processes in the upper atmosphere and the Sun-Earth environment. To this end we examine changes in the amplitudes of the geomagnetic daily variation and activity indices as derived from geomagnetic observatories around the world with records extending back to 1900. One obstacle to extracting long-term trends is the dominant role of the solar cycle in the behaviour of these quantities. Since the solar cycle length is variable, care must be taken when removing its effect to reveal longer-term trends. We compare two different techniques for removing the variable solar-cycle signal: a method developed by Lockwood and Fröhlich (2007) that uses a range of running mean periods; and a simple wavelet analysis. We also compare these techniques to a simple 11-year running mean and comment on the robustness of the results.

Motivation

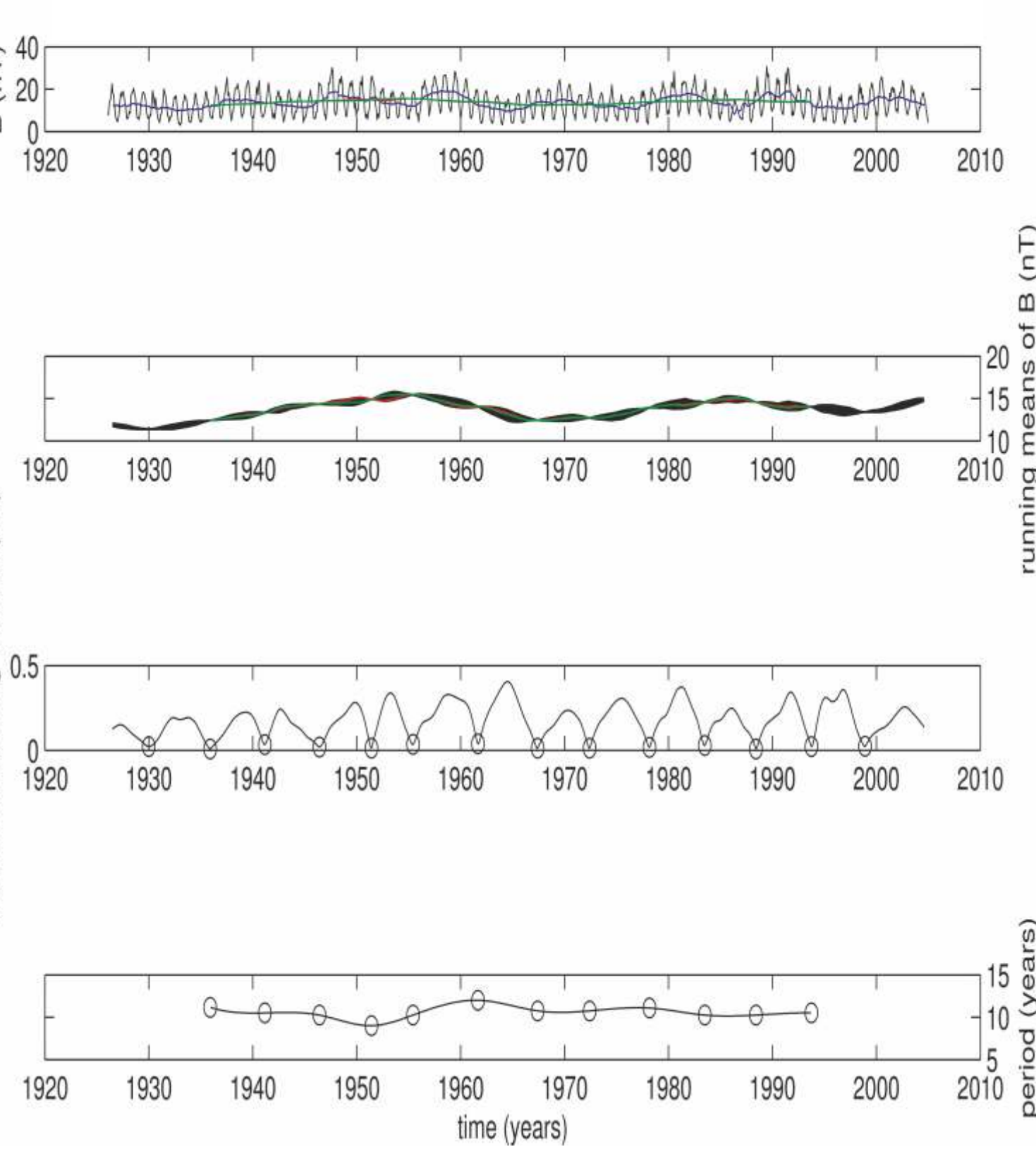
Long-term trends in magnetic activity levels as characterised by, for example, the aa index (Clilverd et al, 1998), inter-hourly variations (Svalgaard et al, 2004) and daily ranges of hourly mean values (Le Mouél et al, 2005) all contribute to understanding long-term changes in the Sun and near-Earth environment. These changes may have important impacts on climate studies. Here we concentrate on the regular magnetic daily variation, Sq, generated in the ionospheric dynamo, a region only 100-150 km from the Earth's surface.

Method

To generate the required time-series, we fit Fourier series (with periods 24, 12 and 8 hours) to hourly mean values from 5 quiet days per month at 15 observatories at mid and low latitudes with time series exceeding 70 years. Their locations are shown to the right.



We then trial two methods of removing the quasi-periodic solar cycle variations from the time-series: Lockwood & Fröhlich (2007) (henceforth LF), and a simple wavelet analysis following Torrence & Compo (1998). Below we show an example of applying each method to Y component data from Hartland.



Lockwood & Fröhlich method (left)

Top panel: Take time series (black curve) and remove annual & semi-annual signals (giving blue curve).

2nd panel: compute running means between 9 and 13 years at each time-step (black curve).

3rd panel: calculate standard deviations of running means at each time step then find minima in these standard deviations.

Bottom panel: derive estimate of solar cycle period from the time between minima in 3rd panel. Fit cubic spline to interpolate periods over whole time-series.

Recompute running means at each time step using periods derived from cubic spline (red curve, 1st and 2nd panels)

Wavelet method (right)

Top panel: take time series (black dots) and remove annual & semi-annual signals (giving black curve).

Middle panel: compute Morlet wavelet power spectrum for periods between 6 and 16 years.

Bottom panel: determine frequency of peak power in 6-16 year period range over the time-series and use this as estimate of the solar-cycle period.

Recompute running means at each time step using periods derived from wavelet power spectrum blue & green curve in top panel).

Black curve in middle panel indicates points in finite time-series where edge effects begin to degrade power spectrum. In period estimation (bottom panel), green part is within unaffected time-series, blue is within affected times but still usable, and red is too close to the edge to compute running mean. In our analysis we use the green and blue parts of the period estimation.

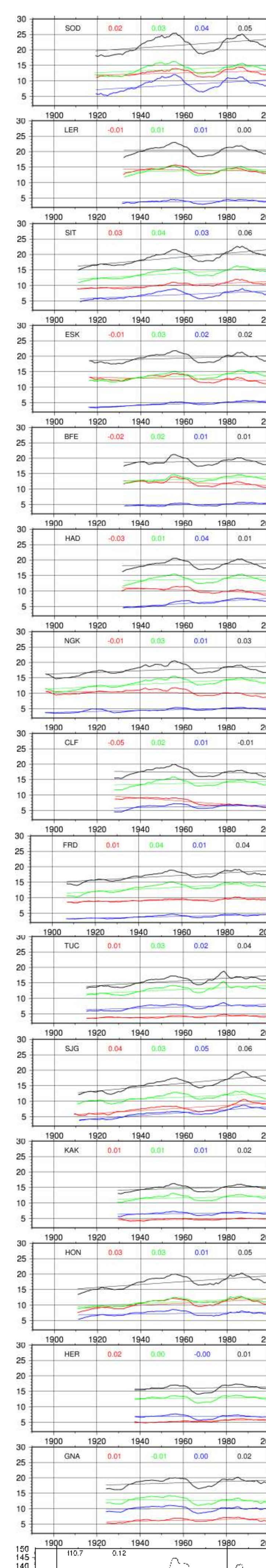
Comparison of LF and wavelet methods

Using synthetic data, the wavelet method produced the lowest RMS misfit between desired signal and recovered signal: ~15% lower than LF and ~60% lower than fixed 11-year running mean.

The wavelet method was easier to automate than LF, where standard deviation minima could be difficult to find in noisy data.

Because of the continuous nature of the wavelet transform, the solar cycle periods could be determined over a wider span of the time-series than was usually the case for LF, where discrete minima in standard deviations determined extent of period estimation.

Results and Interpretation



Shown left are the wavelet-filtered monthly estimates of amplitudes (nT) of geomagnetic daily variations in X (red), Y (green), Z (blue) and F (black) at the selected geomagnetic observatories, ordered by geomagnetic latitude. Also shown in the bottom three plots are (in order) the filtered- f10.7 flux, Ap index, and aa index. In each plot a trend line is fitted to each curve and the gradients (units/year) are given in the corresponding colour. An average of the observatory trends using the wavelet, LF, and 11-year running mean methods is summarised in the table below.

Observatory	Geomagnetic Longitude	Latitude	Years of data Start	End	Mean trend nT/year	X	Y	Z	F
SOD	120.4	63.8	1923	2004	0.02	0.03	0.03	0.05	0.05
LER	89.4	62.1	1927	2004	-0.01	0.01	0.01	0.01	0.00
SIT	279.2	60.3	1890	2004	0.03	0.04	0.03	0.06	0.06
ESK	84	60	1927	2004	-0.01	0.04	0.03	0.02	0.02
BFE	98.7	55.5	1914	2004	-0.03	0.02	0.01	0.00	0.00
HAD	80.3	54	1905	2004	-0.03	0.00	0.05	0.00	0.00
NGK	97.8	51.9	1926	2004	-0.01	0.04	0.02	0.03	0.03
CLF	85.8	49.9	1909	2004	-0.05	0.01	0.01	-0.01	-0.01
FRD	352.9	48.8	1905	2004	0.01	0.04	0.01	0.04	0.04
TUC	315.3	40.2	1901	2003	0.01	0.03	0.02	0.04	0.04
SGJ	5.7	28.7	1919	2004	0.04	0.03	0.05	0.06	0.06
KAK	208.3	27	1911	2004	0.01	0.01	0.00	0.01	0.01
HON	269.2	-21.6	1905	2004	0.04	0.04	0.01	0.05	0.05
HER	83.4	-33.9	1932	2004	0.02	0.01	0.00	0.01	0.01
GNA	188.5	-42.4	1913	2004	0.01	-0.01	0.00	0.03	0.03

Maxima in the 1950s and 1980s are seen in all datasets and all components.

Differences between trends using Lockwood and Fröhlich procedure, 11-year running mean, and wavelet method are ~ 0.01 nT/year, which gives us confidence in the general trends shown. The trend in the Z component is either zero or positive at all observatories. For the Y component, the trend is positive with the exception of GNA. The X component is more variable with positive and negative trends at different observatories. There does not seem to be any obvious pattern in the trends when ordered by geomagnetic latitude, except perhaps in the X component, which is predominantly negative at high latitudes and positive at mid and low latitudes, although the sample is small.

The Ap and aa indices show the same peaks in the 1950s and 1980s as the Sq amplitudes. The length of the aa time-series allows us to see another peak in the 1890s. The length of the Ap time-series is too short to derive a meaningful trend but the longer aa index shows a trend of ~ -0.1 nT/year.

External causes - changes in solar irradiance spectrum

The main cause for the patterns in the magnetic data appears to be related to changes in the solar irradiance spectrum in the EUV band. The upward trend agrees with that in the Sun's coronal magnetic field strength found by Lockwood et al (1999) from the aa index. This index has the daily variation accounted for in its derivation so it therefore characterizes the irregular activity which is a consequence of particle radiation from the Sun.

Internal causes - effects of changes in core-generated field on ionosphere

During the 20th century there has been a decrease in the internal field, in both the dipolar and whole magnetic field as modelled at the surface of the Earth.

Decreasing B should increase both the Hall and Pedersen conductivities and so increase the magnitude of the Sq current as seen from the ground.

It is also likely that the coupling of solar energy into a dipolar magnetosphere would be reduced with a decrease in the dipole but that the increase in its variability (i.e. becoming more quadrupolar, shown above) may increase the occurrence of conditions which favour reconnection with the interplanetary magnetic field (Vogt et al, 2004).

The different trends of the components of Sq could also be a result of the changes in the main field as the directions of the Hall and Pedersen conductivities are orientated by the electric and magnetic fields in the ionosphere. Changes in the main field could shift the pattern of conductivities affecting each component differently.

Acknowledgments and references

Wavelet software was provided by C. Torrence and G. Compo, and is available at URL: <http://atoc.colorado.edu/research/wavelets/>

We thank the staff at the institutes involved in operating the observatories whose data were used in this study, the World Data Centres who collate and distribute them and the producers of the F10.7 dataset.

We acknowledge the support of NERC-funded consortium **GEOSPACE**

Ciliverd, M. A., T. D. G. Clark, E. Clarke and H. Rishbeth, 1998. Increased magnetic storm activity from 1868 to 1995, *J. Atmos. Solar-Terr. Phys.*, **60**, 10, 1047-1056.

Le Mouél, J.-L., Kossobokov, V. and Courtillot, V., 2005. On long-term variations of simple geomagnetic indices and slow changes in magnetospheric currents: The emergence of anthropogenic global warming after 1990? *Earth Planet. Sci. Lett.*, **232**, 273-286.

Lockwood, M. and Fröhlich, C., 2007. Recent oppositely directed trends in solar climate forcings and the global mean surface air temperature, *Proceedings of The Royal Society A*, **463**, 2447-2460.

Lockwood, M., Stamper, R. and Wild, M. N., 1999. A doubling of the Sun's coronal magnetic field during the past 100 years. *Nature*, **399**, 437-439.

Svalgaard, L., Cliver, E. W. And Le Sager, P., 2004. IHV: A new long-term geomagnetic index. *Adv. Space Sci.*, **34**, 436-439.

Torrence, C. and Compo G., 1998. A practical Guide to Wavelet Analysis. *Bulletin of the American Meteorological Society*, **79**, 61-78.

Vogt, J., B. Zieger, A. Stadelmann, K.-H. Glassmeier, T.J. Gombosi, K. C. Hansen, and A. J. Ridley, 2004. MHD simulations of quadrupolar paleomagnetospheres, *J. Geophys. Res.*, **109**, A12221, doi:10.1029/2003JA010273.

